UNIVERSITY OF LEEDS

This is a repository copy of *Coherent three-dimensional terahertz imaging through self-mixing in a quantum cascade laser*.

White Rose Research Online URL for this paper:
http://eprints.whiterose.ac.uk/76884/

Article:
Dean, P, Valavanis, A, Keeley, J et al. (11 more authors) (2013) Coherent three-dimensional terahertz imaging through self-mixing in a quantum cascade laser. Applied Physics Letters, 103 (18). 181112. 181112-1 . ISSN 0003-6951

https://doi.org/10.1063/1.4827886

Reuse
Unless indicated otherwise, fulltext items are protected by copyright with all rights reserved. The copyright exception in section 29 of the Copyright, Designs and Patents Act 1988 allows the making of a single copy solely for the purpose of non-commercial research or private study within the limits of fair dealing. The publisher or other rights-holder may allow further reproduction and re-use of this version - refer to the White Rose Research Online record for this item. Where records identify the publisher as the copyright holder, users can verify any specific terms of use on the publisher's website.

Takedown
If you consider content in White Rose Research Online to be in breach of UK law, please notify us by emailing eprints@whiterose.ac.uk including the URL of the record and the reason for the withdrawal request.

White Rose university consortium
Universities of Leeds, Sheffield & York

eprints@whiterose.ac.uk
https://eprints.whiterose.ac.uk/

Coherent three-dimensional terahertz imaging through self-mixing in a quantum cascade laser

Paul Dean,[1,a)] Alex Valavanis,[1] James Keeley,[1] Karl Bertling,[2] Yah Leng Lim,[2] Raed Alhathlool,[1] Siddhant Chowdhury,[1] Thomas Taimre,[3] Lianhe H. Li,[1] Dragan Indjin,[1] Stephen J. Wilson,[2] Aleksandar D. Rakić,[2] Edmund H. Linfield,[1] and A. Giles Davies[1]
[1]*School of Electronic and Electrical Engineering, University of Leeds, Leeds LS2 9JT, United Kingdom*
[2]*School of Information Technology and Electrical Engineering, The University of Queensland, St. Lucia, Queensland 4072, Australia*
[3]*School of Mathematics and Physics, The University of Queensland, St. Lucia, Queensland 4072, Australia*

(Received 30 August 2013; accepted 16 October 2013; published online 30 October 2013)

We demonstrate coherent terahertz (THz) frequency imaging using the self-mixing effect in a quantum cascade laser (QCL). Self-mixing voltage waveforms are acquired at each pixel of a two-dimensional image of etched GaAs structures and fitted to a three-mirror laser model, enabling extraction of the amplitude and phase parameters of the reflected field. From the phase, we reconstruct the depth of the sample surface, and we show that the amplitude can be related to the sample reflectance. Our approach is experimentally simple and compact, and does not require frequency stabilization of the THz QCL. © *2013 AIP Publishing LLC*.
[http://dx.doi.org/10.1063/1.4827886]

Over the past decade, the quantum cascade laser (QCL)[1] has established itself as one of the most promising radiation sources for imaging applications[2–6] at terahertz (THz) frequencies. The appeal of these semiconductor devices derives from their compact size, broad spectral coverage (∼1–5 THz),[3,7] and high output powers.[8] These attributes, coupled with their ability to generate coherent continuous-wave emission with quantum noise-limited linewidths[9] make THz QCLs particularly suited to the development of coherent THz imaging systems. Nevertheless, owing to the reduced experimental complexity involved, the majority of systems reported to date have employed incoherent detection schemes including the use of microbolometer arrays,[3] Golay cells,[4] and cryogenically cooled bolometers.[2,5] A number of approaches have, though, been taken to demonstrate coherent imaging, including exploiting the heterodyne mixing between a QCL and a local oscillator (LO) derived from a gas laser,[10] and more recently through electro-optic harmonic sampling of the THz field using a near-infrared fs-laser comb.[11] In each of these cases, however, owing to the phase/frequency sensitivity of THz QCLs to thermal and current fluctuations, the QCL was electronically stabilised to the LO in order to enable coherent detection of the THz field. Whilst providing a high signal-to-noise ratio, such locking and stabilisation schemes ultimately result in complex and expansive experimental systems.

An alternative coherent detection scheme that can be realised in an extremely simple and compact configuration exploits the self-mixing (SM) effect in THz QCLs.[6,12] In this approach, radiation from an external target is re-injected into the laser cavity. This leads to interference ("mixing") with the intra-cavity field, causing changes in both the measured optical output power and the laser terminal voltage (voltage variation is proportional to output power variations as the laser is driven from a current source).[13–15] These measureable parameters depend upon both the amplitude and the phase of the reflected radiation field. As such, in this scheme, the THz transmitter, local oscillator, mixer, and detector are all combined in a single laser.

In this work, we exploit the coherent nature of SM interferometry to demonstrate three-dimensional (3D) profiling of exemplar structures using a THz QCL. Interferometric waveforms are acquired by monitoring the QCL voltage under feedback from the THz field reflected from the surface of etched semiconductor samples, while the surface is scanned by a mechanical XY stage. By fitting these waveforms to a steady-state three-mirror laser model, we can map the phase of the reflected field across the two-dimensional (2D) surface, thereby enabling 3D reconstruction with a depth-resolution far less than the radiation wavelength. We also show that the waveform amplitude can be related to the reflectance of the sample surface. This approach is experimentally compact, does not require locking/stabilisation of the laser frequency, and potentially offers high signal-to-noise and fast acquisition, ultimately limited by the picosecond timescales of inter-subband transitions. The SM scheme is also inherently confocal, allowing high transverse resolutions to be attained.[6] Compared to visible/near-infrared approaches, our system benefits from reduced sensitivity to submicron-scaled surface roughness, by virtue of the long radiation wavelength, and also benefits from the ability to interrogate samples and subsurface features concealed by THz-transparent materials and layers.

The imaging system used in this work was based on that described in Ref. 6. The THz QCL consisted of a 10-μm-thick bound-to-continuum[16] active region emitting at ∼2.65 THz ($\lambda \sim 113\,\mu$m), which was processed into a semi-insulating surface-plasmon ridge waveguide with dimensions 3 mm × 140 μm. The device was cooled using a continuous-flow helium cryostat and maintained at a constant temperature of 25 K. A dc power supply was used to drive the laser at a constant current of 1050 mA, just above the lasing

a)Electronic mail: p.dean@leeds.ac.uk

 © 2013 AIP Publishing LLC

[This article is copyrighted as indicated in the abstract. Reuse of AIP content is subject to the terms at: http://scitation.aip.org/termsconditions. Downloaded to] IP: 129.11.176.166 On: Wed, 30 Oct 2013 16:25:03

threshold. Radiation from the laser was focused onto the sample using a pair of 2-in.-diameter f/2 parabolic reflectors, with the mean distance between the laser facet and the target being $L_0 = 41$ cm through an unpurged atmosphere. The THz beam was chopped at a frequency of ~200 Hz and coupled back into the laser cavity along the same optical path as the incident radiation. The SM signal was observed electrically through the laser voltage using an ac-coupled differential amplifier with × 100 gain that was monitored using a lock-in amplifier synchronised to the mechanical modulation frequency. For image acquisition, the sample was raster-scanned in two-dimensions, normal to the THz beam, using computer-controlled translation stages. In addition, the sample was mounted on a third translation stage enabling longitudinal scanning of the sample along the beam path (z-axis) at each transverse position.

Initially, high-resolution 2D images of conical samples fabricated from polytetrafluoroethylene (PTFE) were acquired to demonstrate the surface-profiling capability of our SM approach. Figure 1(a) shows an image of a 2-in.-diameter cone with an angle of elevation of $4.6° \pm 0.4°$, measured using a calliper, in which the magnitude of the lock-in signal is plotted. In this case, a pixel size of 100 μm was used and no longitudinal scanning of the sample was undertaken. Concentric fringes corresponding to a $\lambda/2 = 57\ \mu$m change in depth are clearly visible. By applying a 2D fast Fourier transform to this image, as shown in Fig. 1(b), the fringe spacing d can be obtained from the radius of the dominant annulus in reciprocal space. The angle of elevation of the cone, ϕ, can then be inferred via the relation $\tan(\phi) = \lambda/2d$. In this case, a value of $\phi = 4.7° \pm 0.4°$ is obtained,

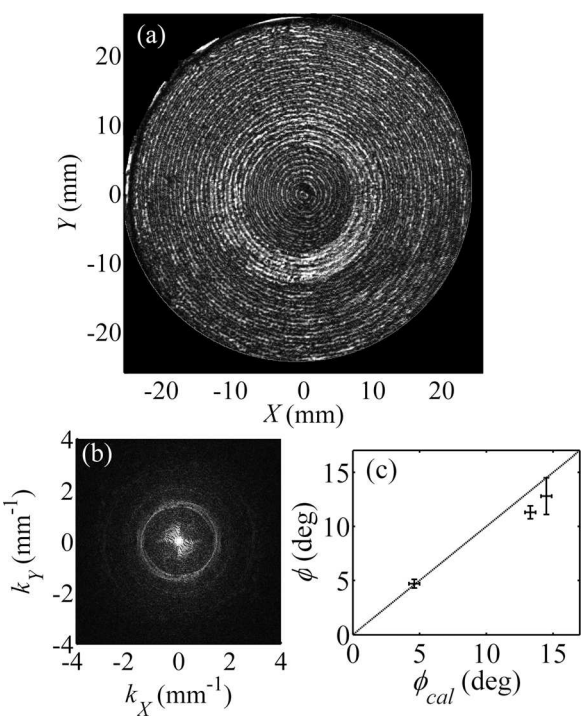

FIG. 1. (a) THz SM image of a PTFE cone with an angle of elevation of $4.6° \pm 0.4°$, showing concentric fringes arising from the slope of the cone surface. (b) 2D Fourier transform of (a). (c) Angle of elevation ϕ inferred from THz SM images for three different cone geometries. The solid line represents $\phi = \phi_{cal}$.

in excellent agreement with that measured using a calliper. Figure 1(c) shows the relationship between the angles measured using a calliper (ϕ_{cal}) and those obtained from the SM images for a range of different cone geometries. As can be seen, excellent agreement is obtained, demonstrating the applicability of our technique for measuring the surface angle/tilt of samples.

In previous heterodyne approaches to coherent cw THz imaging, the phase and amplitude of the reflected THz wave have been encoded in the in-phase and quadrature components of the lock-in amplifier output, for which the reference signal is derived from an electrical beat signal at the intermediate frequency between the THz source and LO.[11,17] Alternatively, the THz wave has been resolved coherently through sampling in the time-domain using an optical delay stage.[18] In our system, the SM waveform can be acquired coherently on a pixel-by-pixel basis by scanning the sample longitudinally, whilst monitoring the instantaneous SM signal via the in-phase component of the lock-in amplifier. It should be noted that the SM waveform could also be acquired by sweeping the laser frequency via modulation of the driving current.[19]

To extract the amplitude of the reflected THz wave from the SM waveforms, as well as the phase accumulation within the external cavity formed by the target, and the feedback parameters, we apply a three mirror model to describe the laser system under feedback,[20] which is equivalent to the steady-state solution to the model proposed by Lang and Kobayashi.[21] In this model, the laser frequency under feedback ω is related to the unperturbed frequency ω_0 through the phase-matching condition

$$\frac{2(L_0 + \delta L)(\omega_0 - \omega)}{c} = C \sin\left(\frac{2(L_0 + \delta L)\omega}{c} + \arctan(\alpha)\right), \tag{1}$$

where L_0 is the nominal external cavity length formed by the remote target, δL is the perturbation to the cavity length arising from the surface geometry of the target, α is the linewidth enhancement factor, and c is the speed of light in vacuum. The feedback parameter C is related to the target reflectance R_{ext}, and other constants including the length, refractive index, and facet reflectivities of the bare laser cavity.[22] The feedback of radiation causes a perturbation to the threshold gain, which in turn produces a modulation of the laser voltage according to

$$\Delta V_{SM} \propto \varepsilon\sqrt{R_{ext}} \cos\left(\frac{2(L_0 + \delta L)\omega}{c}\right), \tag{2}$$

in which ε is a coupling constant representing loss due to attenuation in the external cavity, spatial mode mismatch between the reflected and the cavity mode, and other optical losses due to factors including misalignment and scattering from rough surfaces. Thus, the phase of the SM signal can be related to the distance travelled by the THz radiation in the external cavity, and hence to the depth of the surface of the target δL. Furthermore, the amplitude of the SM waveform can be related to the sample reflectance. It should be noted that Eq. (2) does not describe a purely sinusoidal variation in

[This article is copyrighted as indicated in the abstract. Reuse of AIP content is subject to the terms at: http://scitation.aip.org/termsconditions. Downloaded to] IP: 129.11.176.166 On: Wed, 30 Oct 2013 16:25:03

laser voltage with respect to the external cavity length since the perturbed lasing frequency ω is itself a function of the cavity length via Eq. (1).

Coherent 3D imaging was performed on exemplar GaAs structures that were fabricated by wet chemical etching. Sample A comprised of three stepped regions (in the X-direction) with a nominal step height $\sim$10 μm and a width (in the Y-direction) of 3.1 mm, whereas sample B consisted of five 1.2-mm-wide steps of height $\sim$5 μm. The upper half of each structure was also coated with a 125-nm-thick layer of gold in order to provide regions of differing reflectance. For coherent image acquisition, the sample was scanned on a pixel-by-pixel basis through a longitudinal (z) distance of 0.5 mm, corresponding to nine interferometric fringes. Use of a high sampling resolution of 0.5 μm, corresponding to 1/100 of a fringe, allowed the shape of the fringes to be measured accurately. With a lock-in time constant of 10 ms, the resulting acquisition rate was 20 s/pixel.

Figure 2(a) shows typical SM waveforms obtained from two positions on the surface of sample A corresponding to gold-coated and uncoated regions on different steps, resulting in relative variation in both the phase and amplitude of the waveforms. Also shown are fits to Eq. (2) in which $\varepsilon\sqrt{R_{ext}}$, C, α, and δL are treated as free parameters. Figure 2(b) shows the surface depth δL obtained from the fits to one row of pixels traversing the three stepped regions of sample A (without gold coating). Figures 2(b) and 2(c) also show the average depth variation obtained across all rows (both gold coated and uncoated) for samples A and B, respectively. In each case, the etched steps can be resolved clearly, as can the tilt of the samples, which are estimated to be $\sim$+0.4° and $\sim$–0.2°, respectively. Both samples were then characterised using a non-contact optical profilometer (Bruker NPFLEX 3D), the results of which are included in Figs. 2(b) and 2(c) after correction to replicate the measured sample tilts from the SM signals. As can be seen, there is very good agreement with the THz depth profiles obtained for both samples. The full 3D reconstruction of sample A is shown in Fig. 3(a), in which the colour scale indicates the depth of the surface.

In our technique, the depth resolution is determined by the sampling accuracy of the SM waveforms as well as the frequency instability of the laser caused by temperature and current fluctuations. The first of these influencing factors can be reduced, at the expense of acquisition speed, by longitudinally scanning the sample over a greater distance and with a smaller step-size, and also by applying greater averaging. We can estimate the resolution limit (noise-equivalent displacement[23]) imposed by frequency instability by assuming a typical frequency drift[24,25] $\Delta\omega/2\pi \sim$10–15 MHz over the acquisition period. The resulting phase change of the SM waveform relates to an effective change in cavity length $\Delta L = L_0\Delta\omega/\omega$, which gives a value of $\sim$2 μm in our case, allowing the smaller features of sample B to be resolved. For comparison, the quantum

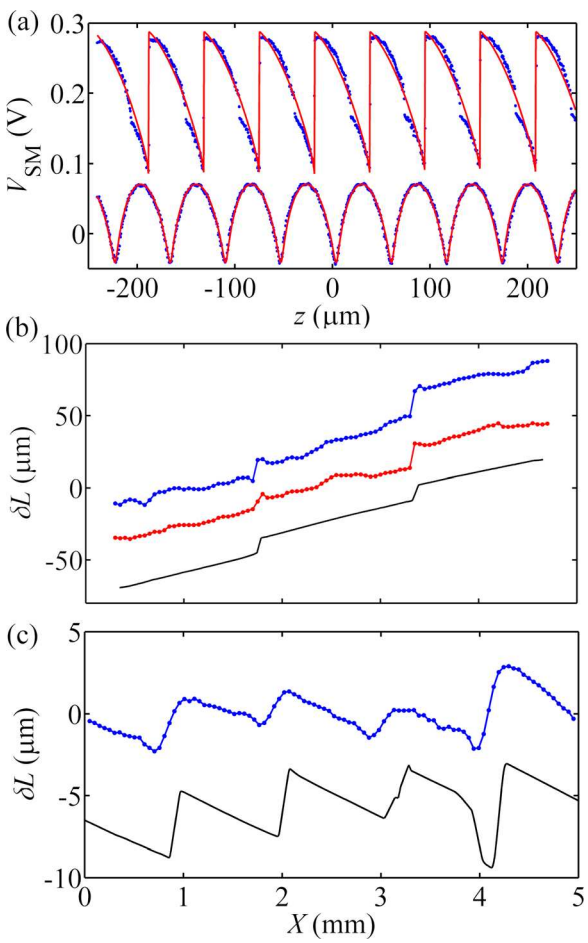

FIG. 2. (a) SM voltage waveforms (blue dots) obtained from two positions on the surface of sample A, and corresponding fits (red solid lines) to Eq. (1). The top trace corresponds to a gold-coated region of the sample. (b) Surface depths δL obtained across one row of pixels A (top trace; blue) and from the average of all rows for sample A (middle trace; red). The horizontal coordinate has been compressed by a factor of 2 for clarity. (c) Surface depths δL obtained from the average of all rows for sample B (top trace; blue). Also shown in both (b) and (c) are the profiles obtained from the non-contact optical profilometer (bottom traces; black solid lines) for samples A and B, respectively. Each trace has been offset vertically for clarity.

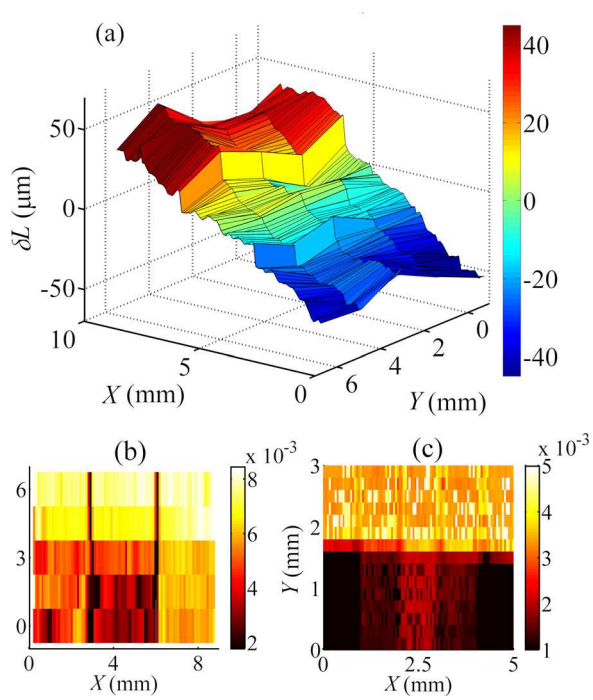

FIG. 3. (a) 3D reconstruction of sample A. (b) and (c) Square of the SM waveform amplitude obtained across the surfaces of samples A and B, respectively. The top region in each image corresponds to the gold-coated region of the sample.

[This article is copyrighted as indicated in the abstract. Reuse of AIP content is subject to the terms at: http://scitation.aip.org/termsconditions. Downloaded to] IP: 129.11.176.166 On: Wed, 30 Oct 2013 16:25:03

noise equivalent displacement is estimated to be $\sim$15 pm, assuming a quantum-limited linewidth of $\sim$100 Hz for this active region scheme.[9] It should also be noted that, based on Ref. 23, speckle-pattern errors for reflection from our semiconductor samples are negligible owing to the small spot-size at the target[6] and the long wavelength compared to surface roughness at terahertz frequencies.

The coherent nature of the SM approach also enables the sample reflectance to be mapped from the amplitude of the SM waveforms, according to Eq. (2). Figures 3(b) and 3(c) show the variation of the square of the fitted waveform amplitude across the surface of samples A and B, respectively. In each case, the top rows of pixels, which correspond to the gold-coated region of the samples, clearly reveal the higher reflectance. However, it can be observed that the amplitude is not homogenous across each region, particularly in the case of sample A. This is attributed to scattering from surface defects and variations in the sample geometry arising from the etching process, which cause deviations in the reflection angle of the beam and hence variation in the coupling constant ε across the surface. Nevertheless, the ratios of the parameters $\varepsilon\sqrt{R_{ext}}$corresponding to the coated and uncoated regions are measured to be 1.28 and 1.61 for samples A and B, respectively. For comparison, assuming complete reflection from the gold layer and a refractive index of 3.6 for GaAs, the expected ratio is 1.77, based on the Fresnel coefficient alone.

In conclusion, we have reported coherent THz imaging using a simple and compact system that exploits the SM effect in a QCL without the need for frequency stabilisation. By extracting the phase and amplitude parameters of a set of SM voltage waveforms, we have demonstrated that this technique allows both the depth and reflectance to be mapped across the surface of structures, with a depth resolution $\sim$2 μm.

The authors acknowledge support from the EPSRC (UK), the ERC "NOTES," and "TOSCA" programmes, the Royal Society and the Wolfson Foundation, and the European Cooperation in Science and Technology (COST) Action BM1205. This research was supported under Australian Research Council's Discovery Projects funding scheme (DP 120 103703). Y.L.L. acknowledges support under the Queensland Government's Smart Futures Fellowships programme. The authors also thank Adrian Eagles, University of Leeds, for assistance with the optical profilometry.

[1]R. Kohler, A. Tredicucci, F. Beltram, H. E. Beere, E. H. Linfield, A. G. Davies, D. A. Ritchie, R. C. Iotti, and F. Rossi, Nature **417**, 156 (2002).
[2]J. Darmo, V. Tamosiunas, G. Fasching, J. Kröll, K. Unterrainer, M. Beck, M. Giovannini, J. Faist, C. Kremser, and P. Debbage, Opt. Express **12**, 1879 (2004).
[3]A. W. M. Lee, Q. Qin, S. Kumar, B. S. Williams, Q. Hu, and J. L. Reno, Appl. Phys. Lett. **89**, 141125 (2006).
[4]K. L. Nguyen, M. L. Johns, L. F. Gladden, C. H. Worrall, P. Alexander, H. E. Beere, M. Pepper, D. A. Ritchie, J. Alton, S. Barbieri, and E. H. Linfield, Opt. Express **14**, 2123 (2006).
[5]P. Dean, N. K. Saat, S. P. Khanna, M. Salih, A. Burnett, J. Cunningham, E. H. Linfield, and A. G. Davies, Opt. Express **17**, 20631 (2009).
[6]P. Dean, Y. L. Lim, A. Valavanis, R. Kliese, M. Nikolić, S. P. Khanna, M. Lachab, D. Indjin, Z. Ikonić, P. Harrison, A. D. Rakić, E. H. Linfield, and A. G. Davies, Opt. Lett. **36**, 2587 (2011).
[7]C. Walther, M. Fischer, G. Scalari, R. Terazzi, N. Hoyler, and J. Faist, Appl. Phys. Lett. **91**, 131122 (2007).
[8]B. S. Williams, S. Kumar, Q. Hu, and J. L. Reno, Electron. Lett. **42**, 89 (2006).
[9]M. S. Vitiello, L. Consolino, S. Bartalini, A. Taschin, A. Tredicucci, M. Inguscio, and P. D. Natale, Nat. Photonics **6**, 525 (2012).
[10]A. A. Danylov, T. M. Goyette, J. Waldman, M. J. Coulombe, A. J. Gatesman, R. H. Giles, X. Qian, N. Chandrayan, S. Vangala, K. Termkoa, W. D. Goodhue, and W. E. Nixon, Opt. Express **18**, 16264 (2010).
[11]M. Ravaro, V. Jagtap, G. Santarelli, C. Sirtori, L. H. Li, S. P. Khanna, E. H. Linfield, and S. Barbieri, Appl. Phys. Lett. **102**, 091107 (2013).
[12]S. Donati, Laser Photon. Rev. **6**, 393 (2012).
[13]S. Donati, *Electro-Optical Instrumentation: Sensing and Measuring With Lasers* (Prentice Hall, New Jersey, 2004).
[14]Y. L. Lim, R. Kliese, K. Bertling, K. Tanimizu, P. A. Jacobs, and A. D. Rakić, Opt. Express **18**, 11720 (2010).
[15]G. Giuliani and S. Donati, *Unlocking Dynamical Diversity: Optical Feedback Effects on Semiconductor Lasers* (John Wiley & Sons, Chichester, 2005).
[16]S. Barbieri, J. Alton, H. E. Beere, J. Fowler, E. H. Linfield, and D. A. Ritchie, Appl. Phys. Lett. **85**, 1674 (2004).
[17]T. Löffler, T. May, C. am Weg, A. Alcin, B. Hils, and H. G. Roskos, Appl. Phys. Lett. **90**, 091111 (2007).
[18]I. S. Gregory, W. R. Tribe, B. E. Cole, C. Baker, M. J. Evans, I. V. Bradley, E. H. Linfield, A. G. Davies, and M. Missous, Electron. Lett. **40**, 143 (2004).
[19]A. D. Rakic, T. Taimre, K. Bertling, Y. L. Lim, P. Dean, D. Indjin, Z. Ikonic, P. Harrison, A. Valavanis, S. P. Khanna, M. Lachab, S. J. Wilson, E. H. Linfield, and A. G. Davies, Opt. Express **21**, 22194 (2013).
[20]K. Petermann, *Laser Diode Modulation and Noise* (Kluwer Academic, New York, 1991).
[21]R. Lang and K. Kobayashi, IEEE J. Quantum Electron. **16**, 347 (1980).
[22]G. Acket, D. Lenstra, A. D. Boef, and B. Verbeek, IEEE J. Quantum Electron. **20**, 1163 (1984).
[23]S. Donati, G. Martini, and T. Tambosso, IEEE J. Quantum Electron. **49**, 798–806 (2013).
[24]S. Barbieri, J. Alton, H. E. Beere, E. H. Linfield, D. A. Ritchie, S. Withington, G. Scalari, L. Ajili, and J. Faist, Opt. Lett. **29**, 1632 (2004).
[25]D. Rabanus, U. U. Graf, M. Philipp, O. Ricken, J. Stutzki, B. Vowinkel, M. C. Wiedner, C. Walther, M. Fischer, and J. Faist, Opt. Express **17**, 1159 (2009).

[This article is copyrighted as indicated in the abstract. Reuse of AIP content is subject to the terms at: http://scitation.aip.org/termsconditions. Downloaded to] IP: 129.11.176.166 On: Wed, 30 Oct 2013 16:25:03